WITHDRAWN: Ultra-Precision Polishing Method of Polymer-Derived Amorphous SiAlCN Ceramics

Yigao Chen

chenyigao321@mail.nwpu.edu.cn

Northwestern Polytechnical University https://orcid.org/0000-0002-1409-6774

Yejie Cao

Northwestern Polytechnical University

Yiguang Wang

Beijing Institute of Technology

Research Article

Keywords: Polymer-derived ceramics, Chemical–mechanical polishing, Polishing defect, Oxidation

Posted Date: August 26th, 2020

DOI: https://doi.org/10.21203/rs.3.rs-63994/v1

EDITORIAL NOTE:

The full text of this preprint has been withdrawn by the authors while they make corrections to the work. Therefore, the authors do not wish this work to be cited as a reference. Questions should be directed to the corresponding author.

Abstract

The amorphous and heterogeneous microstructures of polymer-derived ceramics (PDCs) make it challenging to uniformly polish them without the appearance of obvious polishing defects. In this study, the surface characteristics of polymer-derived silicoaluminum carbonitride (SiAlCN) ceramics were investigated after mechanical polishing and chemical–mechanical polishing (CMP). The results showed the generation of polishing defects including scratches, pits, and comet tails after mechanical polishing; nonetheless, the surface quality was largely improved after CMP, providing an ultra-smooth surface (Ra = ~0.25 nm). The evolution of the surface morphology was characterized in detail and X-ray photoelectron spectroscopy was used to analyze the characteristics of chemical bond before and after the CMP. The polishing slurry dominated the corrosion process during CMP, inducing the oxidation of the SiC_xN_y phase; nonetheless, the so-formed oxidation products and carbon phase were removed by mechanical action. The obtained ultra-high smooth surface can promote practical application in the field of PDCs-based sensors.

1. Introduction

Polymer-derived ceramics (PDCs) have various potential applications in the fields of semiconducting sensors and micro-electromechanical systems due to their outstanding properties, including high temperature stability, corrosion and oxidation resistance, semiconducting properties, and piezoresistive properties [1–4]. However, the performance of PDC-based sensors and their potential applications in the semiconductor industry depend highly on the key requirement of having a high-quality defect-free surface with low surface roughness [5]. Unfortunately, the improvement of the surface quality of PDCs has not been extensively focused upon. To date, a variety of ultra-precision polishing methods such as fluid polishing [6, 7], electrochemical polishing [8], and chemical–mechanical polishing (CMP) have been applied to obtain high-quality defect-free ceramic surfaces [5, 9]. Among them, CMP is considered to be a powerful fabrication technology for removing material by combining chemical and mechanical action together, leading to the achievement of global planarization and ultra-smooth surfaces with no defects [5, 10]. Moreover, it has been widely applied in the fabrication of semiconductor devices and planarization of materials such as silicon-on-insulators [11], sapphire [12], and silicon carbide (SiC) [13]. Therefore, CMP is considered as a potentially important technology to smooth the surfaces of PDCs.

It has been acknowledged that during CMP, effective removal of material is attributed to the mechanical action among the workpieces, pad, and abrasive as well as the chemical action among the workpieces, abrasive, and slurry [5]. Therefore, both the microstructure of the workpieces and the nature of the polishing slurry play an important role in CMP. As a representative PDCs, the polymer derived silicon carbonitride (SiCN) ceramic is composed of the amorphous SiC_xN_y phase and the free-carbon phase [1, 14]. The SiC_xN_y phase supports most of the load in indentation, while the free carbon supports the load in elastic deformation stage [15, 16]. The special heterogeneous microstructure makes the uniform removal extremely difficult, thus leading to the difficulty in acquiring ultra-smooth surface. Thus, appropriate selection of polishing slurry is significantly important as it can provide a unique polishing environment

between the workpieces and the polishing pad, involving both chemical and mechanical action for better polishing, and leading to high efficiency and selective removal [17]. Polishing slurries are usually composed of abrasives, oxidizer, pH regulator, and solvent [5, 10]. For glass and silicon nitride (Si_3N_4) ceramic workpieces, CMP has been successfully applied by using water solution, under polishing environment with pH 7–9, and abrasive with a hardness of approximately 7 Mohs (such as zirconia (ZrO_2) and ceria) [18]. In SiCN ceramics, the SiC_xN_y ceramics phase seems to present a primary contribution to mechanical property on the whole [15, 19]. Therefore, similar polishing slurry was used to assess the underlying CMP mechanisms for polishing SiCN-based PDCs.

Herein, owing to the enhancement of the compactness and oxidation resistance with the addition of aluminum (Al) element [20], the Al-doped SiCN ceramics (SiAlCN) was selected as the target material. The SiAlCN ceramic wafers were first mechanically polished, and then CMP was successfully applied on the pre-polished SiAlCN ceramic wafers using self-made ZrO_2 slurry. Furthermore, the surface morphology and surface roughness were assessed and measured, the formed etching pits were carefully studied, and finally the polishing mechanism for amorphous SiAlCN ceramics was successfully derived.

2. Experimental

SiAlCN ceramic precursors were fabricated based on procedures reported in previous studies [21, 22]. SiAlCN ceramics wafers with a diameter of 9 mm and thickness of ~ 0.5 mm were obtained after pyrolysis at 1000 °C for 2 h in inert gas atmosphere. The density and open porosity of SiAlCN ceramic wafers were ~ 2.0 g cm^{-3} and below 1%, respectively, which were obtained through Archimedes method. The wafers were pasted on the surface of epoxy resin blocks, which were embedded in the clamp head of an automatic polisher (EcoMet™ 250 Pro, Buehler, USA). The SiAlCN ceramic wafers were mechanically polished in succession using fixed diamond lapping films with abrasive grain sizes in a sequence of 9, 6, 3, and 1 μm (Beijing Grish Hitech Co., Ltd., China), marked as #9, #6, #3, and #1, respectively. Deionized water was used as the lapping slurry for the mechanical polishing. After each lapping process, the SiAlCN ceramic wafers were ultrasonically cleaned and rinsed with deionized water and compressed air, respectively. The lapping parameters were optimized as follows: The rotation speeds of the clamp head and lapping films were 30 and 60 rpm, respectively, with an applied pressure of 10 N or 5 N lasting from 2 to 20 min. The ceramic wafers polished after #1 lapping film were then used as the original samples for the following CMP processing in this study. The lapping film was then replaced with a Grish polishing pad (Beijing Grish Hitech Co., Ltd., China) and then the polishing slurry for CMP was changed from deionized water to lab-made ZrO_2 slurry using a feeding system. This lab-made ZrO_2 slurry was composed of monoclinic ZrO_2 (< 100 nm; Aladdin, 99.99% metals basis), a pH regulator ($NaHCO_3$), and deionized water. The ZrO_2 concentration was 1 wt.% and the pH was adjusted to ~ 8. The slurry was ultrasonically dispersed for 30 min prior to its use in the CMP process. Based on the optimal mechanical polishing parameters, the parameters for CMP process were set as follows: lapping pressure of 5 N (which corresponded to the minimum values in the polisher machine), rotation speed of clamp head and

polishing pad of 30 and 60 rpm, respectively, with an optimal duration time of 20 min. Finally, the SiAlCN wafers were cleaned with alcohol, deionized water, and compressed air after the CMP process.

Surface morphology of the samples was characterized by optical microscopy (BX51M, Olympus, Japan), optical profiler method (Wyko NT1100, Veeco, USA), and scanning electron microscopy (SEM; Helios G4 CX, FEI, USA) system equipped with energy dispersive X-ray spectroscopy (EDS) system. The surface roughness was measured via atomic force microscopy (AFM; Dimension Icon, Bruker, USA) with a measurement area of 10×10 μm^2 and 5×5 μm^2, respectively. The average surface roughness was calculated through the detection of surface roughness of five different regions. X-ray photoelectron spectroscopy (XPS; Axis Supra, Kratos, England) was used to analyze the chemical bonding states and phase composition of the SiAlCN ceramic wafers before and after the CMP process through Ar ion beam etching. In order to ensure the accuracy of test results after CMP process, the SiAlCN ceramic wafers were ultrasonically cleaned in alcohol and distilled water prior to testing.

3. Results And Discussion

Figure 1 exhibits the optical images of the surface of SiAlCN ceramic wafers sequentially polished with different diamond-fixed abrasive lapping films. The surfaces of SiAlCN ceramic wafers polished with #9 lapping films appeared to be very rough, with numerous micro-holes and pits generated due to material fractures caused by lateral cracks [23], which still existed after being polished with #6 (Figs. 1a and b). Fortunately, the surface of SiAlCN wafer became smooth and presented a mirror state when #3 lapping film was used, though some mechanical scratches and pits were still retained, which could be clearly observed in Figs. 1c and e. The scratches on wafers' surface were produced due to the mechanical action of the abrasives, and the formation of pits was attributed to the indentation caused by abrasive particles or the deep damage caused by previous procedures [24], which could not be avoided even by adjusting the polishing parameters and surface cleaning time. However, dramatic change in the surface morphology was observed when the polishing was carried out with #1, with the generation of the comet tails defects (Figs. 1d and f). Even when the minimum lapping pressure (5 N) was applied, the comet tails defects could not be avoided. It was likely that the SiC_xN_{4-x} phase, which got detached from the substrate was crushed into smaller particles [25, 26], leading to the formation of several small scratches after dark points, as shown in Fig. 1 f. Therefore, sinking appeared at the area of dark points and protrusions appeared behind dark points. Furthermore, some tiny pits (point I) without comet tails still remained on the surface of SiAlCN ceramics, which were related to the material defects existing due to the previous polishing procedure.

The surface morphology of SiAlCN ceramics polished after #3 and #1 lapping films was further detected by AFM and representative surface morphology is presented in Fig. 2. Surface roughness with Ra values of 0.79 ± 0.17 and 1.42 ± 0.49 nm were, respectively, obtained for the #3 and #1 lapping films based on large number of the detected samples. The low surface quality obtained following the use of #3 lapping film was mainly caused by the large amount of deep mechanical scratches with depth close to 10 nm (Figs. 2a and c). In contrast, the low surface quality for sample polished with #1 lapping film was mainly

caused by the formation of small pits (Figs. 2b and d). The small pits presented wide width compared to the deep scratches, and caused the increase of the surface roughness after polishing with #1 lapping film. This phenomenon was found to be related to the defection of comet tails. The Vickers' hardness of SiCN ceramics ranged from 8.3 to 11.3 GPa [27] (equated to a hardness of ~ 6.5–7 Mohs), which was lower than that of the diamond abrasive (~ 10 Mohs). When #1 lapping film or finer diamond abrasives were employed, the pressure stress applied on the surface of SiAlCN ceramics was therefore high enough to induce indentation and small pits, thus decreasing the surface quality. Therefore, it was difficult to polish uniformly by mechanical polishing only, and CMP was applied to further increase the surface quality. Moreover, even though the surface roughness of samples after being polished with #3 was lower than that of samples polished with #1, the deep mechanical scratches (Figs. 2a and c) were difficult to remove during CMP. Thus, samples polished after #1 were selected as the pre-polished samples for the following CMP process.

Figure 3 exhibits the optical and AFM images of the surface of SiAlCN ceramics obtained following the CMP process with the lab-made ZrO_2 slurry. The scratches and comet tails disappeared completely without the formation of obvious defects. Some tiny dark pits observed on the surface (Fig. 3a) were related to the pits which appeared during previous polishing procedures (Fig. 1d), which were not effectively removed by CMP. The result of the AFM images (Fig. 3c) indicated that the surface roughness value Ra was reduced to 0.24 ± 0.09 nm. The maximum surface height difference was about 1 nm as illustrated in Fig. 3d. Under the condition of polishing slurry, except for the mechanical action, it was indicated that chemical reactions also occurred during the CMP process, leading to the formation of an extremely smooth surface. The nature of the chemical action taking place in this complex SiAlCN ceramic structure during the CMP process was therefore assessed.

Figure 4 illustrates SEM morphology of the surface of polished SiAlCN ceramics before and after CMP. After mechanical polishing with #3, the pits induced due to the mechanical action presented small and irregular profile (Fig. 4a), while the surface morphology became smoother with the large decease of apparent pits after being polished with #1 (Fig. 4b). However, after CMP, some pits still remained on the surface of SiAlCN ceramics (Fig. 3a), and the representative morphology is illustrated in Fig. 4d. The formed pits exhibited a circular profile, which was different from that shown in Fig. 4(a). It was mainly attributed to the chemical action during CMP and the orbital motion of polishing head. Figure 4(c) exhibits the change in the content of detected elements, which may reveal this chemical action. The corresponding elemental compositions are listed in Table I. The result of points I and II indicates the enhancement in the intensity of C element and decrease in the intensity of Si and N elements after CMP. It indicates that the Si or N related phases were removed during CMP and the C-related phase was accumulated. This phenomenon was more noticeable in the pits. Comparative analysis of the results of points II, III, and IV indicates that the intensity of C and O element presented a distinct enhancement, while that of Si, N, and Al elements showed a distinct decrease in pits, which was also demonstrated by the EDS mapping shown in Figs. 4(e)–4(i). It was suggested that the polishing slurry was easily accumulated in the pits, which made the chemical action more serious. Therefore, it was believed that the change of

the intensity of elements was related to the oxidation of sample surface and chemical reaction of Si,N-related phase. Moreover, owing to the rapid removal of target material from the pits, the size of pits gradually enlarged with prolonged polishing time, which should be avoided in practical applications.

The XPS spectra of the surface of SiAlCN ceramics obtained before and after CMP with ZrO_2 slurry are shown in Fig. 5, and the corresponding chemical composition is listed in Table II. Clearly, the characteristic peaks of C 1 s and O 1 s were strengthened, whereas those of N 1 s, Si 2p, and Al 2p were weakened after CMP, indicating the increase in the contents of C and O elements after CMP. The chemical composition of O 1 s, C 1 s, N 1 s, and Si 2p showed an obvious variation, respectively, changing from 5.69, 29.63, 21.85, and 41.66 atomic% prior to CMP to 16.52, 41.8, 13.81, and 27.24 atomic% after CMP. In contrast, a small change for Al was observed, from 1.17 to 0.63 atomic%. The variation of the chemical composition obtained from the XPS data was similar to that of EDS data, thus confirming the occurrence of the chemical action during CMP.

Figure 6 illustrates the detailed XPS spectra of Si, Al, C, and N elements present on the surface of SiAlCN ceramic wafers before and after CMP with the ZrO_2 slurry. All XPS spectra were normalized by C 1 s peak (binding energy (BE) = 284.8 eV) to correct the charge accumulation and contamination of hydrocarbons. Prior to CMP, the peaks for the Si–C, Si–N, and Si–O bonds were identified at 100.5, 102.3, and 103.6 eV [28–30], respectively (Fig. 6a), and Si–N bond was the main chemical bond within SiAlCN ceramics [31]. However, after CMP, the content of the Si–C bond showed a slight increase and the content of the Si–N bond was dramatically reduced from 87.27 to 35.35%. Furthermore, the SiO_x and Si_2N_2O bonds were also detected and identified at 101.3 eV [32] and 101.7 eV [33], respectively. The formation of these two types of bonds was related to the breaking and oxidation of Si–N bond based on the nature of the SiC_xN_y structure within SiAlCN ceramics. The content of the C–Si bond (283.4 eV) [34] also increased from 2.91 to 19.08% as observed in the C1s XPS spectra (Fig. 6b), which could be explained based on the polishing environment. The hardness of SiC crystal was ~ 9.2 Mohs, which was difficult to be removed by the mechanical action of the ZrO_2 abrasive (~ 8 Mohs). Thus, the polishing of SiC by CMP is mainly ascribed to the chemical action, and the polishing degree becomes greater if more alkaline pH ranges (> 10) are used along with oxidizer additives such as H_2O_2 and potassium permanganate [35]. Therefore, the Si–C bond could not be easily removed under current slurry environment and remained on the surface of SiAlCN ceramics, inducing the increased content of Si–C bond. Nonetheless, the Si–C originated only from the SiC_xN_y phase and it exhibited little influence on the complete removal of SiAlCN ceramics due to its low absolute content of the Si–C phase.

Figure 6b shows the generation of the C–O (286.7 eV) [36] and C = O (288.2 eV) [37] bonds with the decrease of C–C (285.6 eV) [38] and disappearance of the C–N (287.7 eV) bonds [39], indicating the occurrence of oxidation during CMP. The C = C (284.4 eV) [38] bond dominated after CMP due to its high bond energy of 602 kJ mol^{-1}, compared to the bond energy of 346 kJ mol^{-1} for C–C bond. Herein, the C–C bond was more easily oxidized and removed, showing large decrease of the C–C bond. Other than the oxidation of the Si and C elements, the oxidation behavior was also observed in other elements as well.

Prior to CMP, a sialon structure (Al–N coordination structure) and Al–O bonds were identified at 74.5 and 75.4 eV, respectively [29, 40] (Fig. 6c). During CMP, the sialon structure was destroyed and oxidized, disappearing from the XPS spectra since only the Al–O bond was observed (74.2 eV) [41]. The oxidation of the sialon, C–N, and Si–N bonds was also confirmed by the XPS spectra of N element (Fig. 5d). Sialon, Si–N, and C–N peaks appeared before CMP at 397.9, 398.6, and 400 eV [29, 39, 42], respectively. However, after CMP, Si–N, Si_2N_2O, and NSi_2O bonds associated with the peaks at 397.2, 397.7, and 400 eV [39, 43] were identified, respectively.

The above mentioned results; therefore, indicate that chemical reactions occurred during the entire CMP process, as shown in Fig. 7, involving mainly the SiC_xN_y phase of SiAlCN ceramics. The Si–N bond dominating the SiC_xN_y phase was ruptured and hydrolyzed to SiO_2, releasing NH_3, which was similar to the hydrolysis of Si_3N_4 crystal during CMP [18, 44], as illustrated in Eq. (1). The resultant SiO_2 reacted with water to produce silicic acid dissolved in water, according to Eq. (2) [26]. Between the Si–N and SiO_2 layers, an intermediary Si_2N_2O layer was then formed according to Eq. (3) [45], as confirmed by XPS patterns. As a result, the chemical action of the polishing SiAlCN ceramics through CMP was found to be greatly related to the oxidation of Si–N. Nevertheless, the difference lies in the other structures that existed in amorphous SiAlCN ceramics. Another main phase in SiAlCN ceramics was the free carbon phase, which was partially oxidized into C–O or C = O bond. The removal of carbon phase was mainly attributed to the mechanical polishing during CMP. Other structures with small content, such as sialon and C–N can also be oxidized into relevant oxidation products, generating SiO_2, Al_2O_3, and other oxide structures (for example, containing C–O bond) on the surface of SiAlCN ceramic wafers. Most of the reaction products can be removed by the subsequent mechanical action of the abrasive. The hardness of the abrasive (ZrO_2) is slightly greater than that of SiAlCN ceramics and the formed SiO_2 (~ 7 Mohs) layer and the reaction products. Therefore, mechanical removal could be mild and fine due to their similar hardness, minimizing the damage due to mechanical action. Owing to the softened SiAlCN ceramics surface and mild mechanical polishing, the scratches formed during previous procedure were removed, providing the extremely smooth surface of SiAlCN ceramic wafers with low damage.

$$Si_3N_4 + 6H_2O \rightarrow 3SiO_2 + 4NH_{3(g)} \quad (1)$$

$$SiO_2 + 2H_2O \rightarrow Si(OH)_4 \quad (2)$$

$$Si-N + SiO_2 \rightarrow Si_2N_2O \quad (3)$$

4. Conclusions

Ultra-smooth surfaces were obtained on amorphous and heterogeneous polymer-derived SiAlCN ceramics by the CMP process. A ceramic sample with a roughness Ra of ~ 1.42 nm was obtained after mechanical

polishing along with polishing defects such as scratches and comet tails. However, after the CMP process the roughness decreased to ~ 0.25 nm, showing an ultra-smooth surface. The polishing mechanism was proposed according to the result of EDS patterns and XPS measurement. During CMP, the SiC_xN_y phase was mainly oxidized to SiO_2 and Si_2N_2O, and subsequently removed by mechanical action, and other oxidation products (such as the oxidation products of C–C, C–N) were also removed by mechanical action. The present study provides new insights into the CMP process to achieve ceramics with extremely smooth surface, in particular, for amorphous and heterogeneous ceramics, thus developing the application of PDCs in the semiconductor fields.

Declarations

Acknowledgement

The authors acknowledge the support of the Natural Science Foundation of Shaanxi Province of China [grant number 2019JQ-540]; the Fundamental Research Funds for the Central Universities [grant number 3102019QD0401]; National Key Basic Research Program of China [grant number 2015CB057400].

References

1. Colombo P, Mera G, Riedel R et al (2010) Polymer-derived ceramics: 40 years of research and innovation in advanced ceramics. J Am Ceram Soc 93:1805–1837
2. Liew LA, Zhang W, Bright VM et al (2001) Fabrication of SiCN ceramic MEMS using injectable polymer-precursor technique. Sensor Actuat A-Phys 89:64–70
3. Ma BS, Wang YG, Wang KW et al (2015) Frequency-dependent conductive behavior of polymer-derived amorphous silicon carbonitride. Acta Mater 89:215–224
4. Shao G, Jiang JP, Jiang MJ et al (2020) Polymer-derived SiBCN ceramic pressure sensor with excellent sensing performance. J Adv Ceram 9:374–379
5. Oliver MR (2004) Chemical-Mechanical Planarization of Semiconductor Materials. Springer (Berlin), Heidelberg
6. Zhao J, Huang JF, Wang R et al (2020) Investigation of the optimal parameters for the surface finish of K9 optical glass using a soft abrasive rotary flow polishing process. J Manuf Process 49:26–34
7. Guo HR, Wu YB, Lu D et al (2014) Effects of pressure and shear stress on material removal rate in ultra-fine polishing of optical glass with magnetic compound fluid slurry. J Mater Process Tech 214:2759–2769
8. Yang X, Sun RY, Ohkubo YJ et al (2018) Investigation of anodic oxidation mechanism of 4H-SiC (0001) for electrochemical mechanical polishing. Electrochim Acta 271:666–676
9. Zantye PB, Kumar A, Sikder AK (2004) Chemical mechanical planarization for microelectronics applications. Mat Sci Eng R 45:89–220

10. Cadien KC, Nolan L (2018) Chap. 10-Chemical Mechanical Polishing Method and Practice. In: Krishna S, Dominic S (eds) Handbook of Thin Film Deposition. William Andrew Publishing, New York, pp 317–357
11. Kulawski M, Henttinen K, Suni I et al (2003) A novel CMP process on fixed abrasive pads for the manufacturing of highly planar thick film SOI substrates. Mat Res Soc Symp Proc 767:133–139
12. Xu WH, Lu XC, Pan GS et al (2010) Ultrasonic flexural vibration assisted chemical mechanical polishing for sapphire substrate. Appl Surf Sci 256:3936–3940
13. Shi XL, Pan GS, Zhou Y et al (2014) Characterization of colloidal silica abrasives with different sizes and their chemical–mechanical polishing performance on 4H-SiC (0001). Appl Surf Sci 307:414–427
14. Gregori G, Kleebe HJ, Brequel H et al (2005) Microstructure evolution of precursors-derived SiCN ceramics upon thermal treatment between 1000 and 1400 ^{o}C. J Non-cryst Solids 351:1393–1402
15. Wen QB, Yu ZJ, Riedel R. *The fate and role of in situ formed carbon in polymer-derived ceramics*. *Prog Mater Sci* 2019, *109*: *100623*.
16. Klausmann A, Morita K, Johanns KE et al (2015) Synthesis and high-temperature evolution of polysilylcarbodiimide-derived SiCN ceramic coatings. J Eur Ceram Soc 35:3771–3780
17. Basim GB, Moudgil BM (2002) Effect of soft agglomerates on CMP slurry performance. J Colloid Interf Sci 256:137–142
18. Jiang M, Wood NO, Komanduri R (1998) On chemo-mechanical polishing (CMP) of silicon nitride (Si_3N_4) workmaterial with various abrasives. Wear 220:59–71
19. Stabler C, Celarie F, Rouxel T et al (2019) Effect of composition and high-temperature annealing on the local deformation behavior of silicon oxycarbides. J Eur Ceram Soc 39:2287–2296
20. Wang YG, Fei WF, An LN (2006) Oxidation/corrosion of polymer–derived SiAlCN ceramics in water vapor. J Am Ceram Soc 89:1079–1082
21. Chen YG, Cao YJ, Wang YG et al (2020) Femtosecond laser pulse ablation characteristics of polymer-derived SiAlCN ceramics. Ceram Int 46:9741–9750
22. Chen YG, Cao YJ, Wang YG et al (2020) Fabrication of grooves on polymer-derived SiAlCN ceramics using femtosecond laser pulses. Ceram Int 46:11747–11761
23. Xie ZH, Moon RJ, Hoffman M et al (2003) Role of microstructure in the grinding and polishing of -sialon ceramics. J Am Ceram Soc 23:2351–2360
24. Wang K, Li YZ, Kang RK et al (2010) Generation and removal of pits during chemical mechanical polishing process for MgO single crystal substrate. Appl Surf Sci 256:2691–2699
25. Rebasa N, Dommarco R, Sikora J (2002) Wear resistance of high nodule count ductile iron. Wear 253:855–861
26. Fang L, Gao YM, Zhang Z (1999) Tribology of Si_3N_4 with different glassy phase content sliding against grey cast iron lubricated with water. Wear 225:896–904

27. Janakiraman N, Aldinger F (2010) Indentation analysis of elastic and plastic deformation of precursor-derived Si–C–N ceramics. J Eur Ceram Soc 30:775–785
28. Mitu B, Dinescu G, Dinescu M et al (2001) Multilayer structures induced by plasma and laser beam treatments on a-Si:H and a-SiC:H thin films. Thin Solid Films 383:230–234
29. Hagio T, Takase A, Umebayashi S (1992) X-ray photoelectron spectroscopic studies of β-sialons. J Mater Sci Lett 11:878–880
30. Tanizawa Y, Suzuki T (1995) Effects of silicate ions on the formation and transformation of calcium phosphates in neutral aqueous solutions. J Chem Soc Faraday T 91:3499–3503
31. Frank B, Markus W, Fritz A et al (2004) Solid-state NMR studies of the preparation of Si-Al-C-N ceramics from aluminum-modified polysilazanes and polysilycarbodiimides. Chem Mater 16:919–929
32. Li HF, Dimitrijev S, Sweatman D et al (1999) Investigation of nitric oxide and Ar annealed SiO_2/SiC interfaces by X-ray photoelectron spectroscopy. J Appl Phys 86:4316–4321
33. Finster J, Heeg J, Klinkenberg ED (1990) Chemical and structural order in silicon oxynitrides by methods of surface physics. Prog Surf Sci 35:179–184
34. Delplancke MP, Powers JM, Vandentop GJ et al (1990) Preparation and characterization of amorphous SiC:H thin films. J Vac Sci Technol A 9:93–97
35. Chen GM, Ni ZF, Xu LJ et al (2015) Performance of colloidal silica and ceria based slurries on CMP of Si-face 6H-SiC substrates. Appl Surf Sci 359:664–668
36. Allison DA, Johansson G, Allan CJ et al (2007) Molecular spectroscopy by means of ESCA III. Carbon compounds. J Electron Spectrosc 1:269–283
37. Shen L, Dai JJ (2007) Improvement of hydrophobic properties of silk and cotton by hexafluoropropene plasma treatment. Appl Surf Sci 253:5051–5055
38. Yamamoto K, Koga Y, Fujiwara S et al (1998) Dependence of the sp^3 bond fraction on the laser wavelength in thin carbon films prepared by pulsed laser deposition. Appl Phys A 66:115–117
39. Yamamoto K, Koga Y, Fujiwara S (2001) XPS studies of amorphous SiCN thin films prepared by nitrogen ion-assisted pulsed-laser deposition of SiC target. Diam Relat Mater 10:1921–1926
40. Chang SL, Anderegg JW, Thiel PA (1996) Surface oxidation of an Al-Pd-Mn quasicrystal, characterized by X-ray photoelectron spectroscopy. J Non-Cryst Solids 195:95–101
41. He HY, Alberti K, Barr TL et al (1993) ESCA studies of aluminophosphate molecular sieves. J Phy Chem 97:13703–13707
42. Ingo GM, Zacchetti N, Sala DD et al (1989) X-ray photoelectron spectroscopy investigation on the chemical structure of amorphous silicon nitride (-SiN_x). J Vac Sci Technol A 7:3048–3055
43. Rignanese GM, Pasquarello A, Charlier JC et al (1997) Core-level shifts and microscopic structure. Phys Rev Lett 79:5174–5177
44. Dante RC, Kajdas CK (2012) A review and a fundamental theory of silicon nitride tribochemistry. Wear 288:27–38

45. Komanduri R, Hou ZB, Umehara N et al (1999) A “gentle” method for finishing Si_3N_4 balls for hybrid bearing applications. Tribol Lett 7:39–49

Tables

Table I. The elemental composition of the detected points shown in Fig. 4.

Atom%	Si	Al	C	N	O
I(Before CMP)	42.63	1.54	29.15	19.85	6.83
II(After CMP)	28.88	1.07	46.89	16.24	6.92
III	15.93	0.23	58.41	9.48	15.95
IV	13.39	0.21	58.40	11.36	16.64

Table II. The chemical composition of the polished surface of SiAlCN before and after CMP

Atom%	Si2p	Al2p	C1s	N1s	O1s
Before CMP	41.66	1.17	29.63	21.85	5.69
After CMP	27.27	0.63	41.80	13.79	16.51

Figures

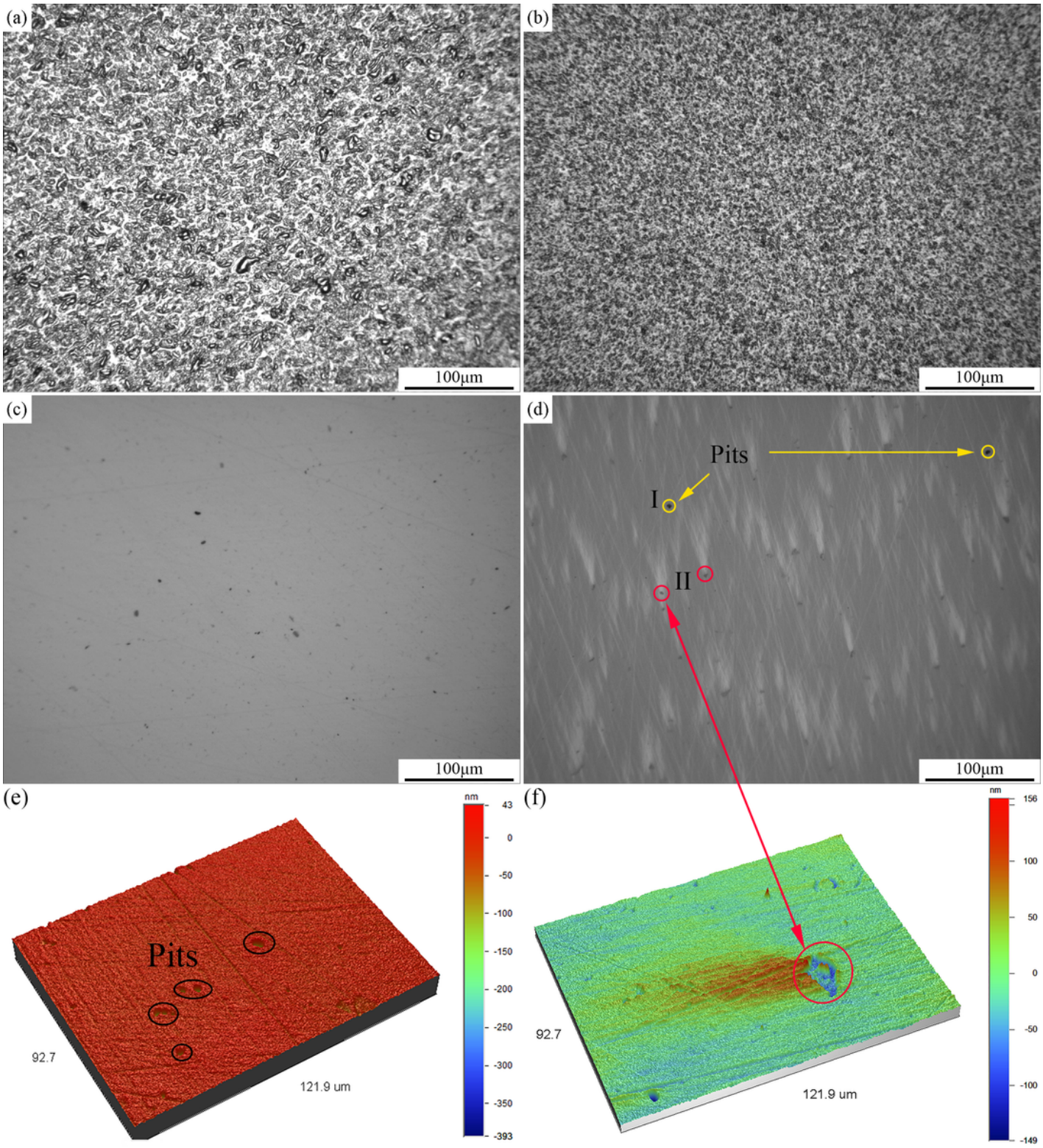

Figure 1

Optical images of the SiAlCN ceramics polished with the lapping film fixed with diamond abrasive of different sizes: (a) 9 μm, #9; (b) 6 μm, #6; (c) and (e) 3 μm, #3; (d) and (f) 1 μm, #1. (e) and (f) exhibit the surface morphology of pits and comet tails, with a measurement area of 92.7 × 121.9 μm2.

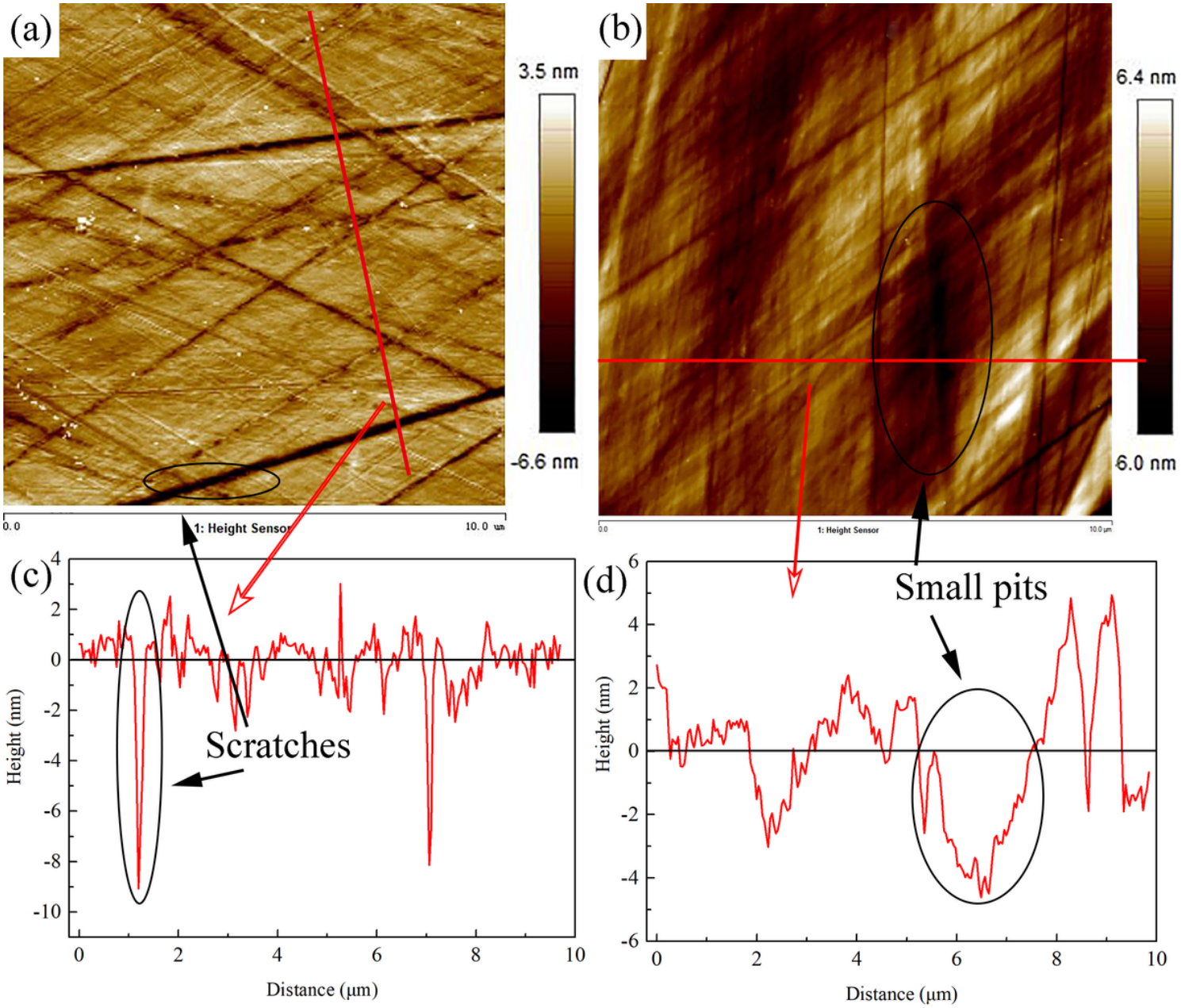

Figure 2

AFM images (10 × 10 µm2) of SiAlCN ceramic wafers polished with different lapping films. (a) #3, (b) #1. (c) and (d) are cross-section images along the lines in (a) and (b).

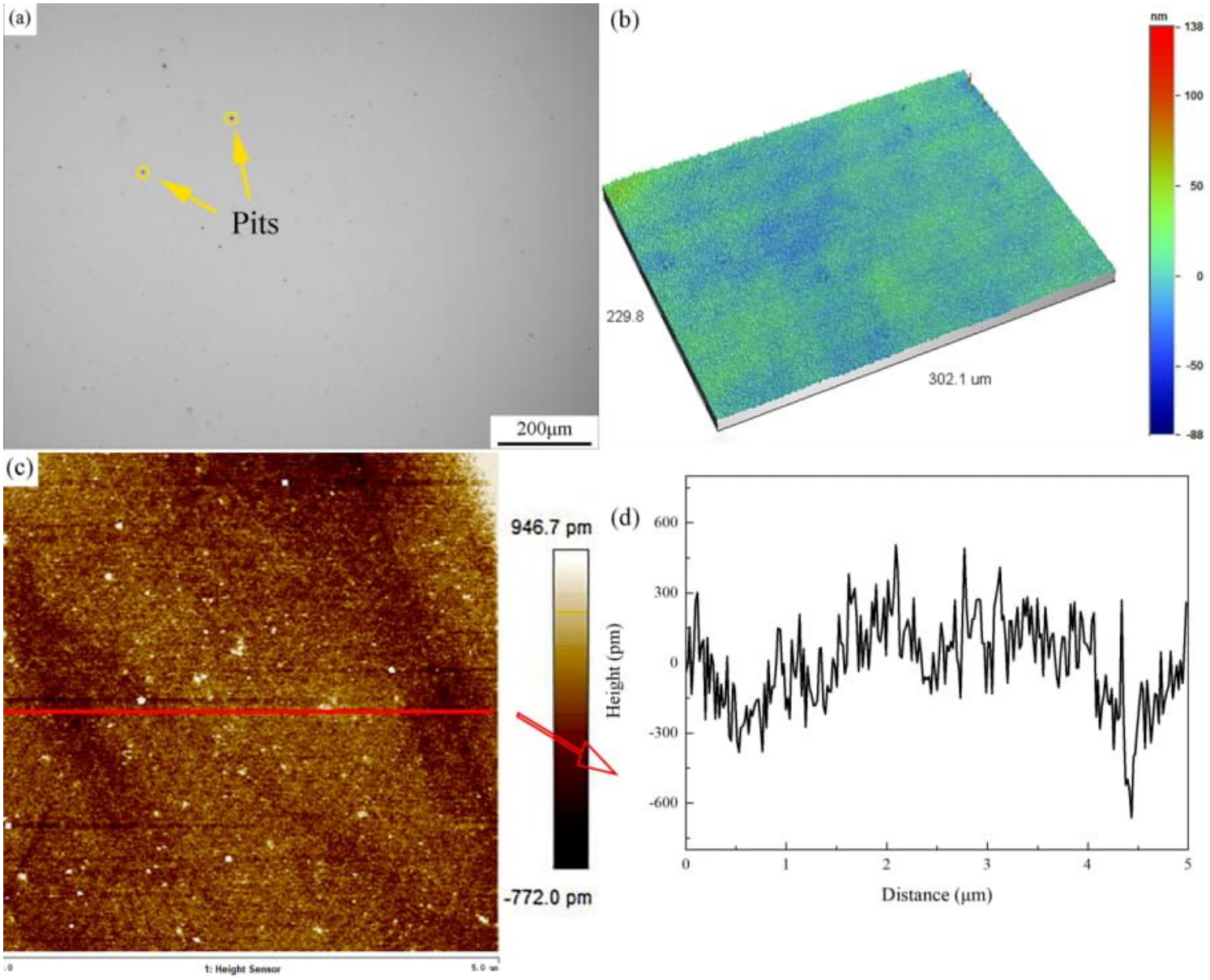

Figure 3

Surface morphology of SiAlCN ceramics after CMP process with the lab-made ZrO2 slurry: (a) and (b) Optical images (c) AFM image (5 × 5 μm2), and (d) Cross-section profile along the lines in (c).

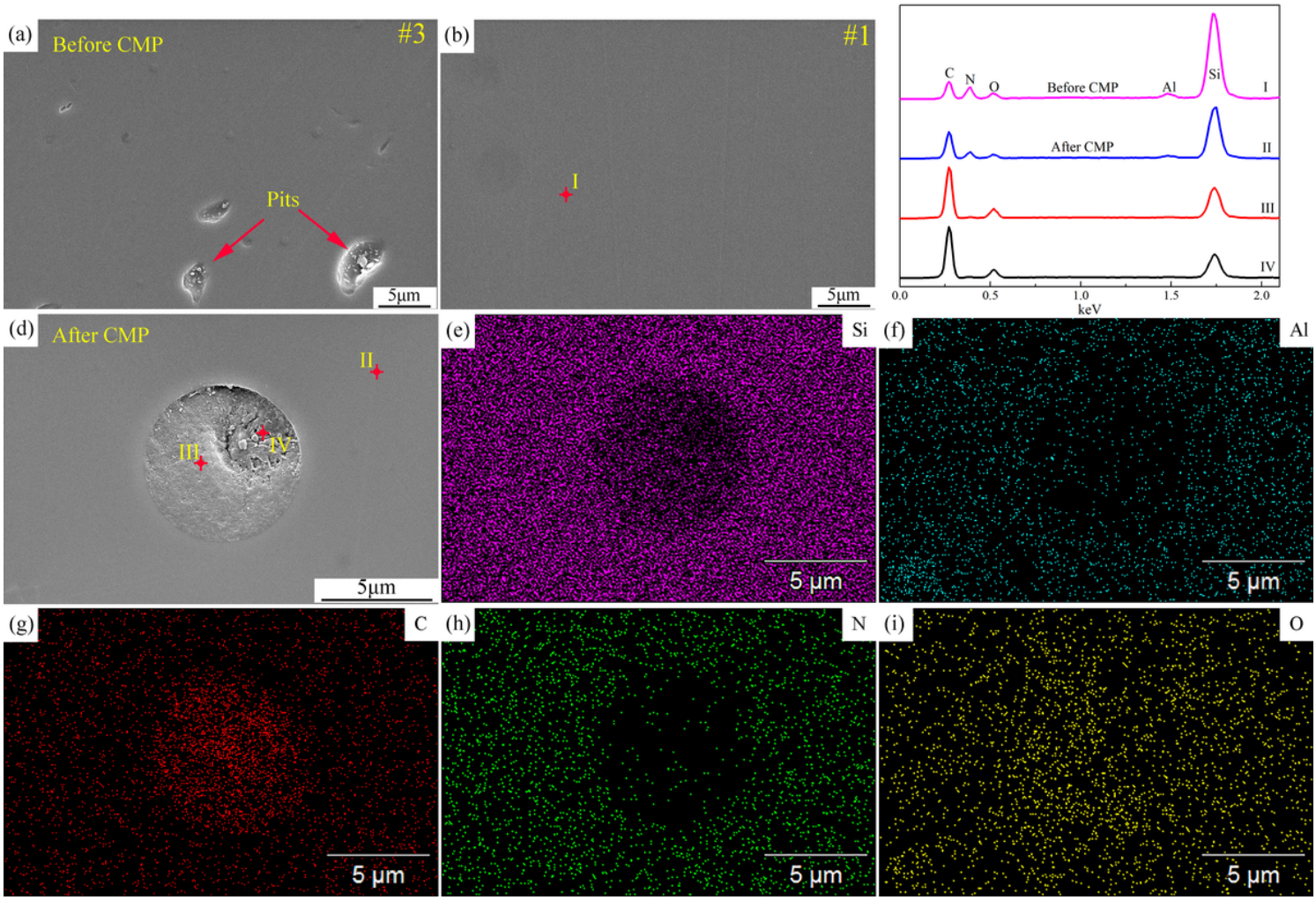

Figure 4

SEM micrographs and EDS patterns of the etched pit when CMP with ZrO2 polishing slurry has been applied. The points in the EDS patterns represent the polishing defects with three detected points, marked as I, II, and III.

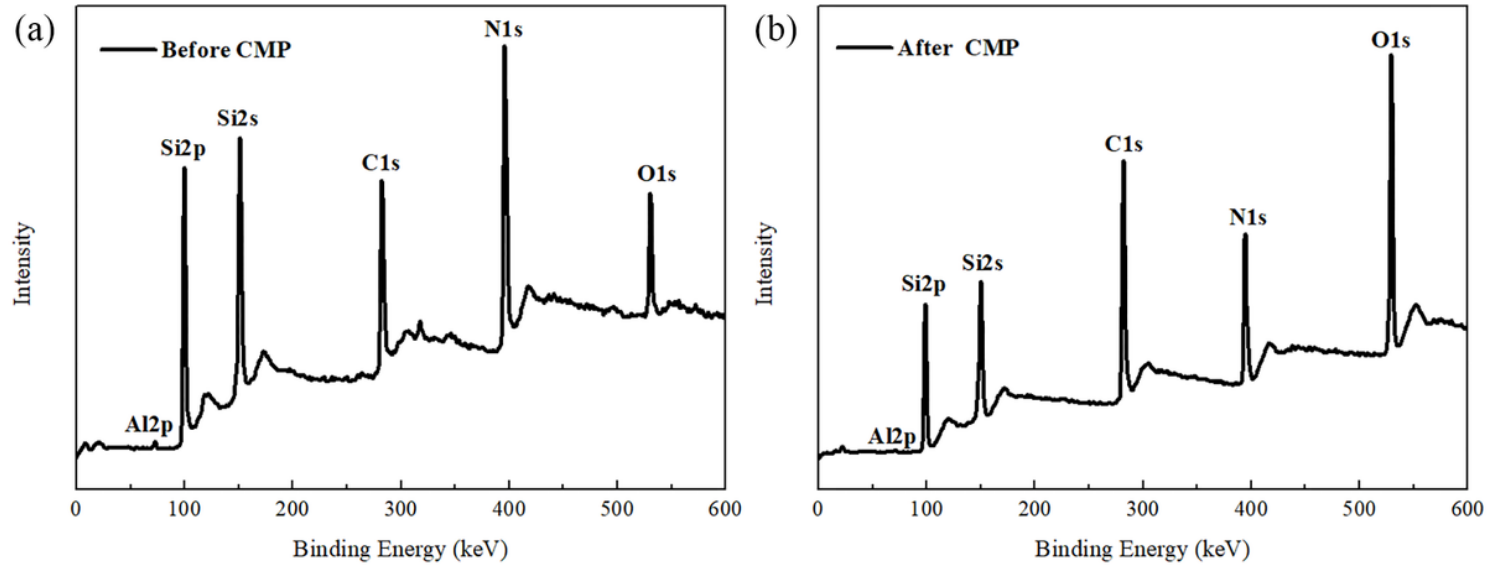

Figure 5

XPS spectra corresponding to the surface of SiAlCN ceramics before and after CMP with ZrO2 slurry.

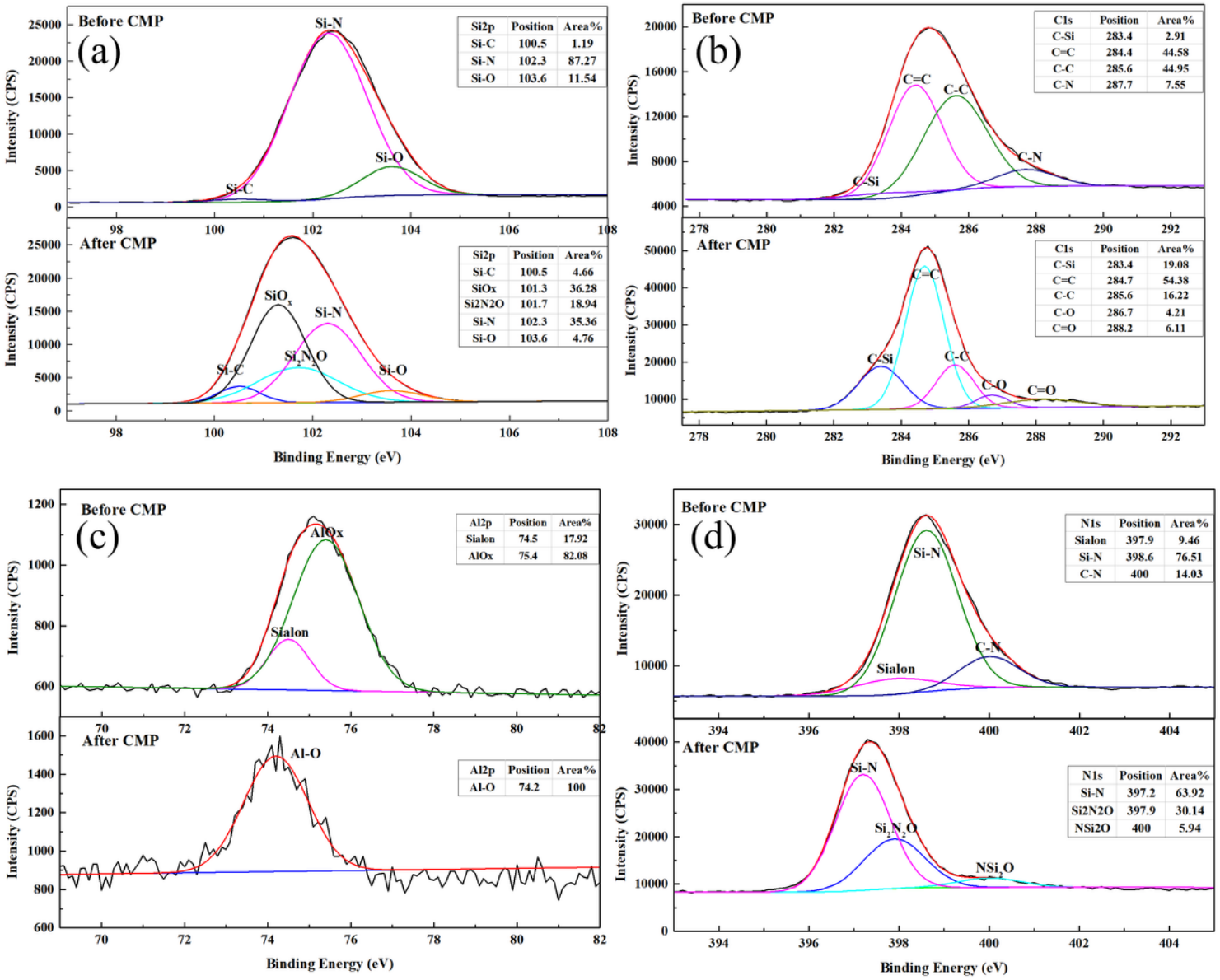

Figure 6

XPS spectra corresponding to the surface of SiAlCN ceramics before and after CMP with ZrO2 slurry. Inset: Table listing the chemical composition (atomic%) calculated from the XPS spectra.

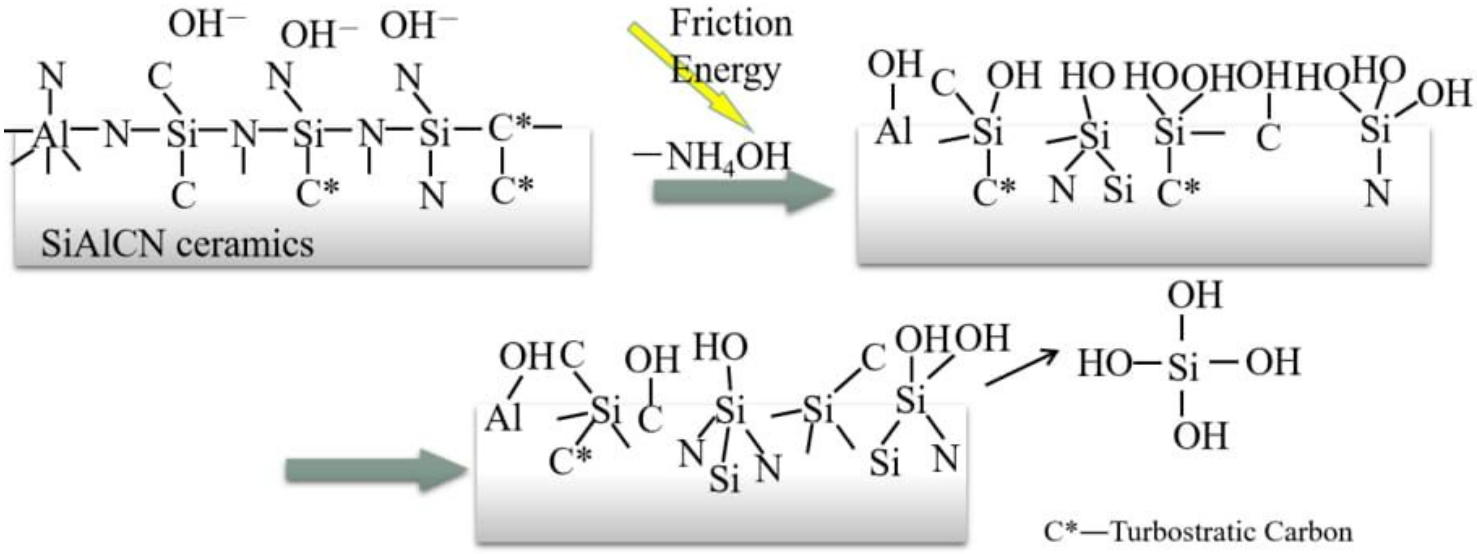

Figure 7

Schematic of oxidation and removal process of SiAlCN ceramic during CMP.